Mössbauer spectrometry of Fe(Cu)MB-type nanocrystalline alloys: II. The topography of hyperfine interactions in Fe(Cu)ZrB alloys

1997 J. Phys.: Condens. Matter 9 2321

(http://iopscience.iop.org/0953-8984/9/10/018)

J. Phys.: Condens. Matter **9** (1997) 2321–2347. Printed in the UK PII: S0953-8984(97)79197-5

Mössbauer spectrometry of Fe(Cu)MB-type nanocrystalline alloys: II. The topography of hyperfine interactions in Fe(Cu)ZrB alloys

Marcel Miglierini† and Jean-Marc Greneche

Laboratoire de Physique de l'Etat Condensé, URA CNRS 807, Université du Maine, F72017 Le Mans Cédex, France

Received 4 November 1996

Abstract. Changes in the microstructure, crystallization behaviour and magnetic state of $Fe_{87.5-x}Cu_xZr_{6.5}$ ($x = 0, 1$) alloys upon annealing for one hour at 500–840 °C are examined by ^{57}Fe Mössbauer spectrometry, x-ray diffraction and differential thermal analysis measurements. The presence of crystallites is reflected in the Mössbauer spectra taken in the temperature range 77 K to 473 K as sharp lines which are superimposed on broad features of the residual amorphous phase. The principal crystalline phase is identified as bcc-Fe. An early stage of crystallization is found even after only a 500 °C/1 h anneal. The total fraction of crystalline phase increases as the temperature is increased. Hyperfine fields of Fe atoms positioned in grain boundaries of the crystallites are affected by the ordered structure of the crystallites from one side, and by the disordered amorphous arrangement from the other. The behaviour of this amorphous/crystalline interface zone is studied by considering two independent hyperfine-field distributions. One is attributed to the interface zone and the other represents the amorphous remainder of the original precursor. The three-dimensional distributions of hyperfine fields obtained from this fitting procedure, which was introduced in part I, the previous paper, enable us—after their decomposition into several gaussian components—to sketch a model of the topography of the hyperfine interactions within nanocrystalline samples.

1. Introduction

Fe-based nanocrystalline materials are becoming important candidates for practical applications [1]. Very good soft magnetic properties were evident in FeCuZrB systems [2] which, depending on the annealing conditions, can exhibit ultra-fine bcc-Fe crystalline grains emerging from the original amorphous precursor. The insoluble constituent elements which are not participating in the crystal growth process remain in the amorphous remainder. The latter seems to govern the magnetic behaviour of the nanocrystalline systems [3, 4] because it enables propagation of ferromagnetic exchange interactions through paramagnetic layers of the amorphous zone to occur [4, 5].

Mössbauer spectrometry is a unique tool for simultaneous study of the short-range-order arrangement, and/or magnetic states of the resonant atoms and their nearest neighbourhoods. The majority of investigations of the Fe(Cu)ZrB nanocrystalline system, however, utilize the information obtained from Mössbauer effect measurements mainly for the characterization of crystalline phases created during thermal treatment and/or to establish the ratio of the

† On leave from: Department of Nuclear Physics and Technology, Slovak Technical University, Ilkovičova 3, 812 19 Bratislava, Slovakia (e-mail:bruno@elf.stuba.sk). This is also the address for any correspondence.

0953-8984/97/102321+27$19.50

volume of the crystalline phase to that of the residual amorphous phase. The feasibility of using Mössbauer spectrometry to probe the immediate surroundings in the investigation of distributed hyperfine interactions has not so far been thoroughly examined, however. This paper attempts to demonstrate how the capability of resonant atoms to unveil the complex behaviour of spins can be thoroughly exploited.

To utilize fully the diagnostic potential of Mössbauer spectrometry, we apply a novel approach to the fitting of Mössbauer spectra of nanocrystals which was introduced in part I, the previous paper [6]. Broadened lines are decomposed into two distributed components with completely independent sets of spectral parameters. Sharp lines are reproduced by a sextet of lorentzian profiles. Using such an approach we can follow the changes which are taking place in the amorphous remainder as well as those in the intermediate region between the amorphous and crystalline phase, with respect to the annealing temperature and temperature of the measurement. This fitting model is also applicable to samples containing small amounts of amorphous phase. Using three-dimensional projections of the distributions obtained, we discuss correlation between the structural short-range-order arrangement and the hyperfine interactions within Fe(Cu)ZrB alloys. Moreover, a detailed analysis of hyperfine-field distributions over a wide range of measuring temperatures and for different stages of crystallization (different annealing temperatures) enables us to design a topography of hyperfine interactions. First of all, however, we would like to give a brief survey of recent Mössbauer effect investigations of the Fe(Cu)ZrB system, and point out the principal achievements.

2. Mössbauer spectrometry for Fe(Cu)ZrB nanocrystalline alloys

Because it provides the possibility of studying both the structural arrangement and the magnetic states of the resonant atoms, Mössbauer spectrometry is frequently employed as a principal and/or additional analytical tool in the characterization of nanocrystalline materials.

Kopcewicz *et al* [7–9] have used radio-frequency (rf) fields to allow them to reach conclusions regarding the size of the α-Fe crystals as a function of annealing temperature. The rf Mössbauer experiments that they performed upon $Fe_{81}Zr_7B_{12}$ and $Fe_{79}Zr_7B_{12}Cu_2$ alloys permit them to distinguish the soft nanocrystalline bcc-Fe phase from the magnetically hard microcrystalline α-Fe phase. These experiments also allowed the determination of the distribution of anisotropy fields as related to the size distribution of the α-Fe grains [7]. A more detailed discussion on the shape of the collapsed spectra of $Fe_{81}Zr_7B_{12}$ as a function of annealing temperature is given in [8]. The Mössbauer spectra presented in [7, 8] were taken only at ambient temperature, with adequate cooling of the samples to prevent excessive heating during the rf exposure.

The magnetic behaviour of the disordered spectral components is discussed in [9], where single-block hyperfine-field distributions are also presented. They show two distinct types of short-range order in the remaining amorphous phase toward higher annealing temperatures. The intensity of the secondary peak in $P(H)$, which appears at about 26.5 T and 29 T for $Fe_{81}Zr_7B_{12}$ and $Fe_{79}Zr_7B_{12}Cu_2$ alloys, respectively, increases with annealing temperature, and it is ascribed to the onset of the Fe_3Zr phase as was speculated on the basis of x-ray diffraction measurements [9]. A large number of Fe atoms appear in the magnetic phases, such as bcc-Fe, Fe_3Zr, and the retained amorphous phase. Fe atoms with zero magnetic field are related to the fcc-Fe phase ascribed to γ-Fe according to the isomer shift values. Annealing at 780 °C causes complete crystallization of the samples studied.

Conversion-electron Mössbauer spectrometry (CEMS) performed upon the same samples [10] revealed enhanced surface crystallization, which starts at lower annealing

temperatures than for the bulk case. In addition, new crystalline phases are detected, corresponding to the tetragonal Fe_2B phase, and are formed exclusively at the surfaces of the samples on both the shiny and the dull sides. The CEMS and transmission Mössbauer spectra were analysed with the NORMOS program, using the combination of the hyperfine-field distribution related to the amorphous phase, and subspectra with discrete values of the hyperfine fields corresponding to the crystalline phases. A spectral component with $H_{\rm eff} \approx 27.5$–29 T found in the spectra resembled that of the interfacial regions in the Fe/Zr compounds, and was attributed to the grain boundary regions between the nanocrystalline bcc-Fe and the amorphous host.

Gorría *et al* [11] employed magnetic and Mössbauer effect measurements to study amorphous and nanocrystalline $Fe_{86}Zr_7Cu_1B_6$ alloys. The temperature dependence of the Mössbauer spectra obtained from the same specimens is reported by Orúe *et al* [12]. The existence of several types of chemical short-range order in the amorphous phase is the main conclusion for as-quenched samples studied at 77, 300, and 360 K. The non-equivalent magnetic sites observed are not directly related to the different chemical environments arising because of the different areas of the corresponding parts of the distributions obtained for different measuring temperatures. The hyperfine parameters of the total amorphous phase in the samples annealed for 1 h at 650 K (∼380 °C) and 720 K (∼450 °C) are reported to remain almost constant, even though some changes are noted for the two Fe sites considered for the amorphous phase.

A double-peak behaviour of the hyperfine-field distributions was found when the samples were annealed at 790 K (∼520 °C) and 870 K (∼600 °C) [11, 12]. It is concluded that there has been a rearrangement which favours the increase of low-field sites at the expense of the high-field ones. The existence of higher hyperfine fields is attributed to Fe_3B and Fe–B crystalline phases in [11] and [12], respectively, without any support from other measurements. Even after extended study of the magnetic and electrical properties of the FeZrB(Cu) system, including the previous $Fe_{86}Zr_7Cu_1B_6$ sample as well as the $Fe_{91}Zr_7B_2$ alloy [13], no progress was made in the interpretation of the Mössbauer data, and the same misleading conclusions regarding the presence of different crystalline phases are again compiled in [14].

Because of smaller value of $H_{\rm eff}$ for the crystalline phase observed for the samples annealed at 650 K and 720 K (32.6 T at 300 K [11, 12]), the crystallites are supposed to be not exactly pure α-Fe phase. It is noteworthy that a small percentage of the α-Fe (2 and 9–10%, respectively [11, 12]) and a considerable portion of their amorphous environment, together with the prevailing electric quadrupolar hyperfine interactions, are responsible for the decreased value of $H_{\rm eff}$, as will be discussed later in this paper. For the higher annealing temperatures of 790 and 870 K, the hyperfine parameters correspond exactly to those of α-Fe [12].

Navarro *et al* [15] have studied $Fe_{88}Zr_7B_4Cu_1$ nanocrystalline alloys obtained after annealing at 500–705 °C/1 h. They present only room temperature Mössbauer spectra which have been analysed using the NORMOS program. The single-block distributions of hyperfine fields derived resemble those in the case of the presence of two magnetically different regions. For the as-cast state, no ferromagnetic phase has been detected. The crystallization process has been found to consist of two steps. In the first step (after annealing up to 500–600 °C), precipitation of α-Fe (47–59%) takes place. The remaining amorphous matrix evolves to a ferromagnetic phase. A non-ferromagnetic phase (5–8%) was also detected. Annealing at more elevated temperatures completely crystallizes the amorphous phase, and three new crystalline components are found. They are related to Fe–Zr and Fe–B phases (20.5% after 705 °C/1 h). The improvement of the soft magnetic properties is

ascribed to the continuous increase in the volume fraction of the α-Fe nanocrystalline phase (73.5% after 705 °C/1 h) and to the compositional changes in the amorphous matrix [15].

Gómez-Polo *et al* [16] have utilized Mössbauer spectrometry and x-ray diffraction to derive additional information about the magnetic hardening of the $Fe_{87.2}Zr_{7.4}B_{4.3}Cu_{1.1}$ alloy. The hardening was shown to be a consequence of the existence of a few nanocrystals of α-Fe which are separated by a distance that on average is longer than the exchange–correlation length of the amorphous matrix. Changes in the magnetic nature of the residual amorphous phase are thought to be responsible for the phenomenon described. Decoupling between the ferromagnetic grains, and thereby the observed magnetic hardening, is attributed to the occurrence of a non-magnetic Fe phase in the partially crystallized samples. The Mössbauer spectra are fitted using three different contributions: a sextet with broad lines represented by a distribution of hyperfine fields attributed to the residual amorphous matrix; the sextet characteristic of the precipitated α-Fe crystalline phase; and a doublet which must be associated with a non-ferromagnetic Fe phase.

Samples prepared from the same Fe(Cu)ZrB master alloys as in the present study were structurally characterized by Duhaj *et al* [17] using the methods of transmission electron microscopy, electron and x-ray diffraction, and resistometry. Results of Mössbauer effect measurements made at 77 K and 300 K are also provided, but they only confirm the existence of two magnetically non-equivalent neighbourhoods of Fe atoms in the amorphous structure of the as-quenched alloys. The characterization of the thermally treated specimens is given only for one annealing temperature (818 K, i.e. 545 °C). Utilizing a single-block $P(H)$ distribution, it is concluded that the amorphous phase has a more heterogeneous structure for FeCuZrB samples than for FeZrB samples as derived from their much less smooth $P(H)$ curves [17].

In our earlier work on $Fe_{87.5-x}Cu_xZr_{6.5}$ alloys [18], we focused our attention on the changes in the chemical and topological short-range order of the residual intergranular phase as a function of the annealing time (at 550 °C) using three-dimensional $P(H)$ distributions. The latter were constructed from single-block hyperfine-field distributions and depicted well separated bimodal profiles like in [9, 11, 12, 14–17]. Average fields and standard deviations of $P(H)$ distributions corresponding to the amorphous remainder, together with their relative contents, are presented as functions of the annealing temperature for a one-hour annealing time as well.

The simple fitting models mentioned above, however, are not able to account properly for the complex arrangement of spins in Zr-containing alloys, especially when crystalline grains of nanometric size are present. This is, perhaps, why changes that are taking place in the amorphous matrix are only claimed to depend on the annealing temperature, but the mechanism responsible is not discussed. We have shown [6] that great care must be taken when interpreting single-block distributions. To support the conclusions derived, several annealing and/or measuring temperatures or conditions of measurements should be employed.

Kopcewicz *et al* [10] introduce an interfacial FeZr component reproduced by a single sextet to account for a spectral feature as mentioned above. Kemény *et al* [19] reported a satellite to the pure Fe contribution in the Mössbauer spectra of Fe(Cu)ZrB alloys which is located at about 30 T, and they ascribed it to Fe atoms in the bcc phase with Zr first neighbours. We would like to note, however, that the same satellite feature of the Fe crystalline components is revealed also in Mössbauer spectra of alloys which do not contain any Zr, e.g., in $Fe_{80}Ti_7Cu_1B_{12}$ [20] and $Fe_{73.5}Nb_{4.5}Cr_5Cu_1B_{16}$ [21] nanocrystals. That is why we have introduced a fitting model which takes into account different structural positions of the resonant Fe atoms [6]. The present work was initiated with the aim of shedding some

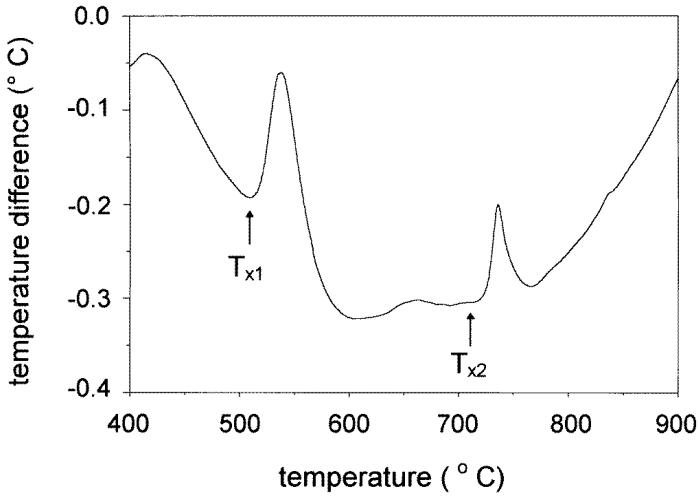

Figure 1. The differential thermal analysis measurement for the $Fe_{86.5}Cu_1Zr_{6.5}B_6$ amorphous alloy. The heating rate was 10 K min^{-1}.

light on the behaviour of the hyperfine interactions of the disordered structural components of Fe(Cu)ZrB nanocrystals utilizing this elaborate advanced fitting procedure.

3. Experimental details

Ribbon-shaped amorphous $Fe_{87.5-x}Cu_xZr_{6.5}$ ($x = 0, 1$) specimens (thickness: $\approx$20 μm; width: 5 and 3 mm, respectively) were prepared by the method of planar-flow casting at the Institute of Physics, Slovak Academy of Sciences, in Bratislava [17]. To obtain different stages of crystallization we performed thermal treatments at 500, 600, 700, and 840 °C each for one hour in a vacuum ($p < 10^{-3}$ Pa). The annealing temperatures were chosen according to the results of the differential thermal analysis given below. The nanocrystalline specimens prepared were subjected to structural characterization carried out using x-ray diffraction data recorded on a Philips diffractometer with Cu Kα radiation. The differential thermal analysis (DTA) was performed under argon using a Setaram thermal analyser. The heating rate was 10 K min^{-1}.

Mössbauer spectra were taken with a standard spectrometer working in a constant-acceleration mode with a ^{57}Co(Rh) source. The temperature of the measurement was chosen in the range 77 K to 448 K for all samples to enable us to investigate the different magnetic arrangements, and to obtain a precise interpretation of the hyperfine interactions and/or a determination of the crystalline fraction content. The samples were placed in an Oxford Instruments bath cryostat during low-temperature (77 K to 300 K) experiments. The above room temperature (from 300 K to 448 K) measurements were done using a home-made vacuum furnace.

A small permanent magnet ($H_{ext} \approx 0.3$ T) was used to ensure parallel orientation of the magnetic moments within the plane, i.e., perpendicular to the γ-beam, for the ribbon-shaped samples in order to reduce the number of free fitting parameters. That is, a fixed line intensity ratio of 3:4:1:1:4:3 was assumed for all of the magnetically split spectral components. A complete set of samples was remeasured at room temperature and the in-field Mössbauer

spectra were utilized to verify the reliability of the fitting procedure employed.

The spectral parameters were refined with the help of the NORMOS DIST program [22] using a procedure described in part I, the previous paper, in more detail [6]. For the above-T_C spectra we have used discrete distributions of quadrupolar splitting values which have been linearly correlated with the isomer shifts of the respective spectral component to account for the spectrum asymmetry. The Mössbauer spectra of the as-quenched specimens were analysed using a single-distribution block of hyperfine magnetic fields (below T_C) and a quadrupolar splitting (above T_C). The isomer shift values are quoted with respect to the spectrum of bcc-Fe at 300 K. We have assumed equal f-factors for the resonant atoms located in the various structural positions when determining their relative contribution to the total spectrum area.

4. Results and discussion

4.1. DTA and x-ray diffraction

The crystallization process for the as-quenched samples was followed by differential thermal analysis in a temperature range from 20 to 980 °C. Figure 1 shows the most important temperature region for the amorphous $Fe_{86.5}Cu_1Zr_{6.5}B_6$ alloy. Two clearly distinct exothermic peaks can be found. They are located at 539 °C and 735 °C, and correspond to the first and to the second crystallization step, respectively. The onset of crystallization is expected at $T_{x1} \approx 500$ °C, at which temperature the partial structural transformation from the amorphous Fe to the bcc-Fe is supposed to take place. Above the second crystallization temperature $T_{x2} \approx 700$ °C the occurrence of other crystalline phases is possible. Our results are similar to those reported for the $Fe_{79}Zr_7B_{12}Cu_2$ alloy [10].

To obtain samples in different stages of crystallization, we have annealed them accordingly to trace the onset of crystallization (500 °C), the temperature region in which the first step of crystallization is partially (600 °C) and fully completed (700 °C), as well as the final stage of crystallization beyond the second exothermic peak (840 °C).

As seen from x-ray diffractograms of the same specimen in figure 2, the first stage of crystallization up to 600 °C is characterized by the occurrence of α-Fe grains only. The presence of small amounts of ZrO_2 (the reflection at about 30°) is revealed for specimens annealed at above this temperature. At 700 °C, still no traces of other Fe-based crystalline phases are seen. Finally, for the sample annealed at 840 °C, an additional set of reflections is observed, and they can be assigned to iron boride and iron–zirconium phases [17]. As is evident from Mössbauer spectrometry, a small amount of the remaining amorphous phase (≈8%) is still found.

4.2. Mössbauer spectrometry

4.2.1. The as-quenched state. Mössbauer spectra of as-quenched $Fe_{87.5-x}Cu_xZr_{6.5}B_6$ alloys taken at various temperatures are shown in figure 3. Their corresponding distributions of hyperfine interactions are illustrated on the right-hand side of each panel. Examples of spectra recorded at 77 K and 300 K, and in the vicinity of the particular ordering temperature of the amorphous matrix are presented in this and in the following figures showing Mössbauer spectra to illustrate the manifestation of hyperfine interactions for different measuring temperatures, and also to enable a comparison to be made of different samples whose spectra were measured at 77 K and 300 K. The values of the isomer shift (with respect to the spectrum of bcc-Fe), the average hyperfine field, and the quadrupolar

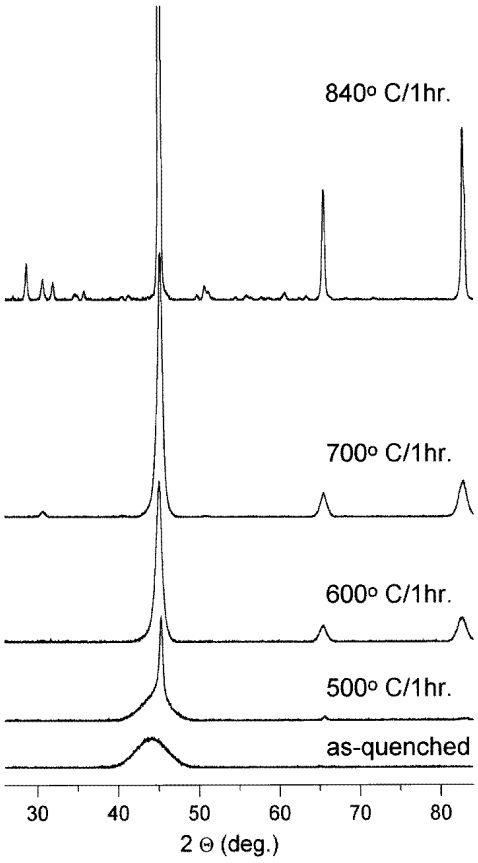

Figure 2. The x-ray diffraction measurement for the $Fe_{86.5}Cu_1Zr_{6.5}B_6$ alloy which was heat treated at the temperatures indicated for one hour in a vacuum.

splitting, as well as standard deviations of the distributions from figure 3, are plotted in figure 4 against the temperature of the measurement. Open circles represent the $x = 0$ sample and the solid ones represent the $x = 1$ sample. The scales of the left-hand and right-hand y-axes in figures 4(b) and 4(c) are directly related to one another, to allow the comparison of the $P(H)$ and $P(\Delta)$ distribution parameters.

The six-line spectra recorded below the magnetic ordering temperature of the as-quenched alloy were reproduced by discrete distributions of hyperfine magnetic fields $P(H)$, linearly correlated with isomer shifts to account for the sextet asymmetry. The distributions $P(H)$ exhibit asymmetrical shapes: this implies the presence of magnetically non-equivalent atomic sites, especially for low magnetic fields. This behaviour is commonly observed for Zr-containing metallic glasses which have rather complex magnetic structure strongly dependent on the Zr content [23, 24].

Nearly identical average values of the isomer shifts in figure 4(a) are evident for both the as-quenched alloys without ($x = 0$) and with ($x = 1$) copper. The addition of Cu, however, causes some changes in the atomic arrangement which are indicated by the elevated hyperfine magnetic fields for $x = 1$ in figure 4(b) (the left-hand y-axis), and by the increased temperature of crystallization as shown in the following section. The

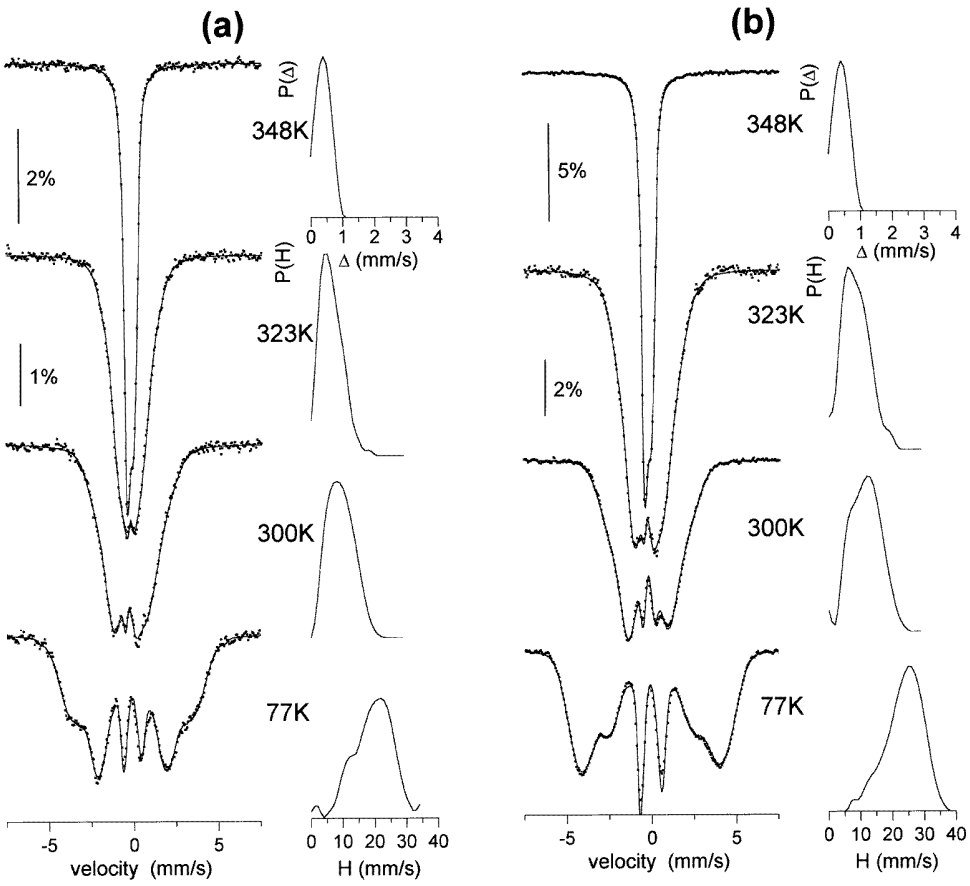

Figure 3. Mössbauer spectra (left in each panel) taken at the temperatures indicated, and the corresponding distributions of hyperfine interactions (right in each panel) of the as-quenched $Fe_{87.5-x}Cu_xZr_{6.5}B_6$ alloys: (a) $x = 0$; (b) $x = 1$.

decrease in the average magnetic field with temperature is associated with a magnetic-to-paramagnetic transformation which is completely achieved at about 330 K and 340 K for $x = 0$ and $x = 1$, respectively. The presence of Fe atoms with a dominating paramagnetic arrangement of spins is revealed already at 300 K, as is evident from the non-zero values of $P(H)$ for $H \rightarrow 0$ T in figure 3.

Above 340 K all of the magnetic interactions vanish completely (figure 3). The paramagnetic spectra have been fitted by distributions of the quadrupolar splitting $P(\Delta)$. The average value of the quadrupolar splitting in figure 4(b) (see also the inset) decreases with the temperature of the measurement, and so does the standard deviation in figure 4(c) (inset). Because standard deviations are related to changes in the short-range-order arrangement, their decrease can be explained in terms of a structural relaxation which favours more ordered atomic arrangement on a short-range level at elevated temperatures. It is noteworthy that the magnetic-to-paramagnetic transition for the as-quenched specimens is well defined and sharp, as seen from both the respective spectra in figure 3 (obvious changes in line shapes and intensities) and from the parameters in figures 4(b) and 4(c) (abrupt changes in the average value and standard deviation).

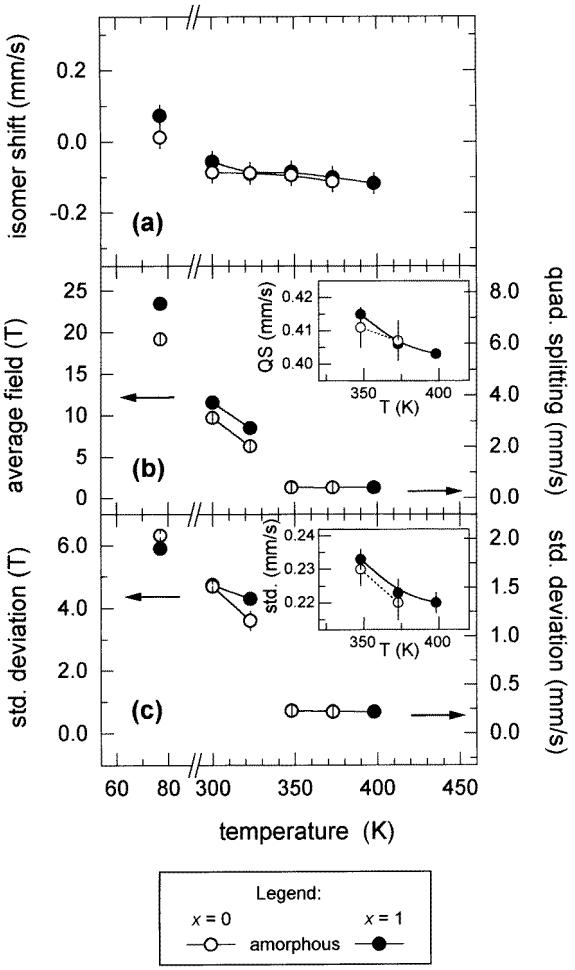

Figure 4. Parameters of the Mössbauer spectra plotted against the temperature of measurement for the as-quenched $Fe_{87.5-x}Cu_xZr_{6.5}B_6$ alloys (open circles: $x = 0$; solid circles: $x = 1$): the isomer shift (a), and the average field (b) and its standard deviation (c).

4.2.2. Before the first stage of crystallization. Figure 5 introduces the Mössbauer spectra of $Fe_{87.5-x}Cu_xZr_{6.5}B_6$ alloys which were each annealed at 500 °C for one hour taken at the temperatures indicated. For $x = 0$, the crystallization has just started, as is seen from the hardly noticeable traces of the magnetically split sextet. This proof of the presence of crystallites is better observed in the spectra taken above room temperature where the central broadened lines, which are assigned to the amorphous remainder, manifest the prevailing electric quadrupolar interactions. The total crystalline fraction is less than 1%. These spectra were fitted by a single distribution $P(H)$ or $P(\Delta)$ and one sextet of lorentzian lines, because the negligible size of the crystalline fraction prevented us from searching also for the interface component.

The addition of Cu decreases the crystallization temperature as seen from the Mössbauer spectra for $x = 1$ in figure 5, where the corresponding sextet of sharp lines is better resolved and even estimation of the interface-zone contribution is possible. The interface atoms are

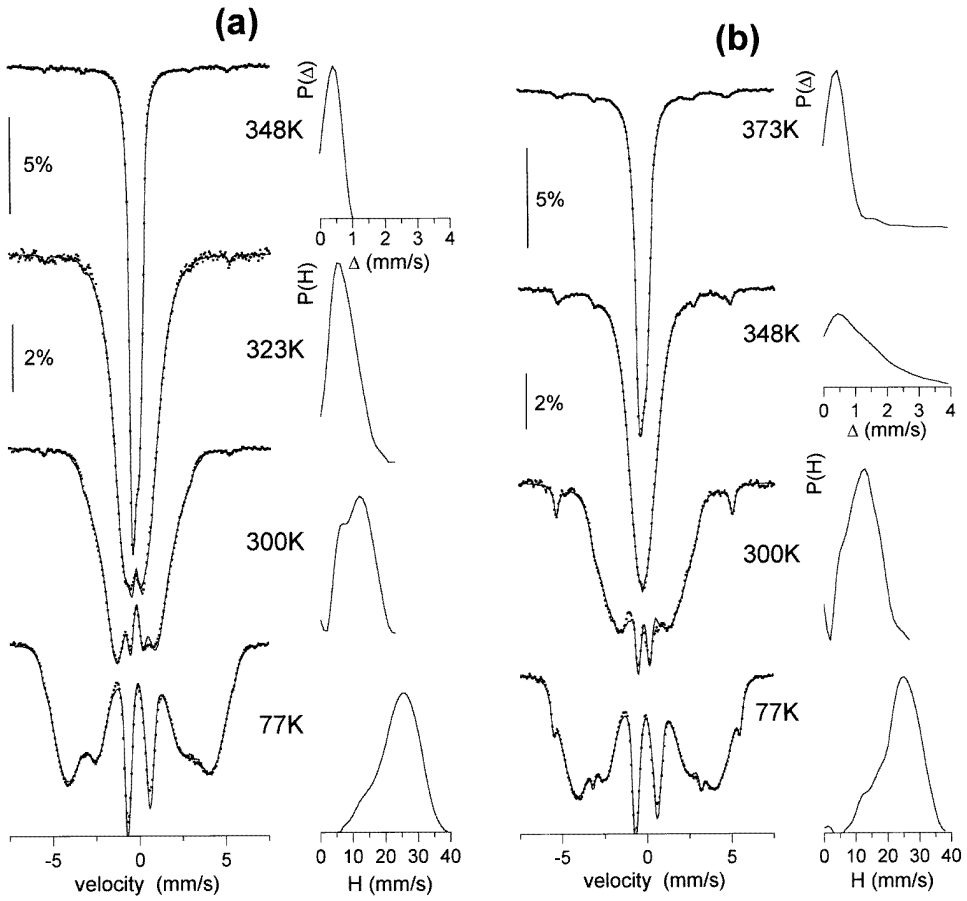

Figure 5. Mössbauer spectra (left in each panel) taken at the temperatures indicated, and the corresponding distributions of hyperfine interactions (right in each panel) of the 500 °C/1 h heat-treated $Fe_{87.5-x}Cu_xZr_{6.5}B_6$ alloys: (a) $x = 0$; (b) $x = 1$.

in this case, however, reproduced by another sextet of lorentzian lines with a rather large linewidth, thus modelling their disordered nature.

The isomer shifts, hyperfine fields, average values and standard deviations of the $P(H)$ and $P(\Delta)$ distributions are plotted against the temperature of measurement in figure 6 as open ($x = 0$) and solid ($x = 1$) symbols: circles represent the amorphous phase (AM), squares stand for the parameters of the interface zone (IF), and triangles denote the crystalline phase (CR).

Even though the contribution of α-Fe nanocrystals in the Mössbauer spectra with $x = 0$ is hardly visible in figure 5(a), it is manifested by the increased average magnetic field of the amorphous remainder at low temperatures in figure 6(b). In addition, an increase in T_C(AM) by about 10 K to ≈340 K and by about 20 K to ≈360 K with respect to that for the as-quenched state is observed for the $x = 0$ and $x = 1$ specimens, respectively.

To explain the increase in T_C(AM) for the amorphous remainder, three essential kinds of origin can be suggested: (i) structural and stress relaxation effects within the amorphous matrix; (ii) a decrease in Fe content in the amorphous remainder; and (iii) the presence of exchange magnetic interactions between crystalline grains and the amorphous matrix.

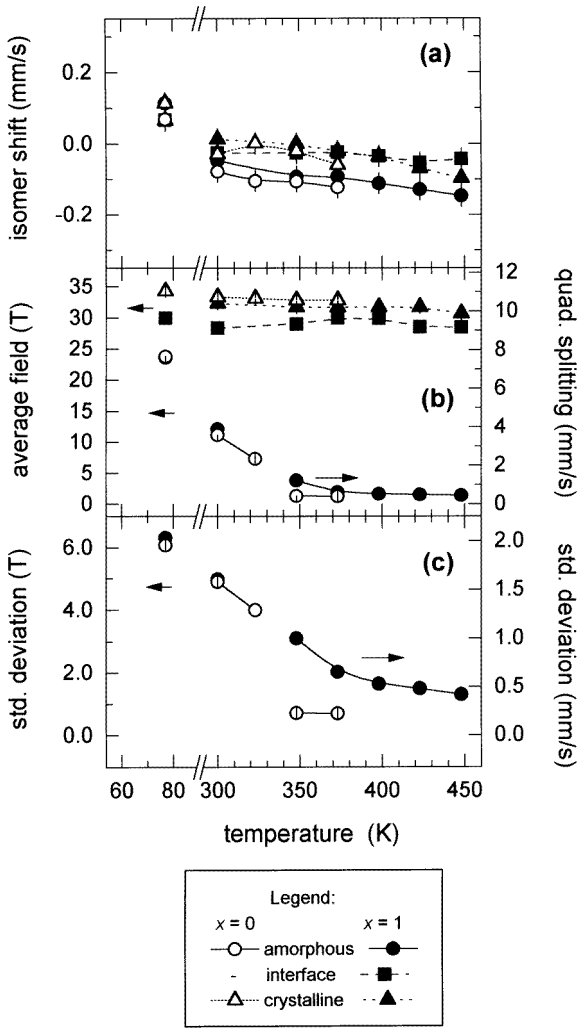

Figure 6. Parameters of the Mössbauer spectrum components (AM—circles; IF—squares; CR—triangles) plotted against the temperature of measurement for the 500 °C/1 h heat-treated $Fe_{87.5-x}Cu_xZr_{6.5}B_6$ alloys (open symbols: $x = 0$; solid symbols: $x = 1$): the isomer shift (a), and the average field (b) and its standard deviation (c).

(i) It is well established that the melt-spinning technique is associated with an inhomogeneous quenching process, inducing a distribution of amorphous states, i.e. of free volumes, associated with the presence of internal stresses and local inhomogeneities, mainly in the case of narrow ribbons (<2 mm). Annealing treatments remove these inhomogeneities and internal stresses, leading to a sizeable increase of the Curie temperature and a slight increase of the average value of the hyperfine field.

(ii) During the devitrification process, iron atoms will migrate to create crystalline grains, inducing a decrease of the iron content within the amorphous remainder. Because of the rather complex magnetic phase diagram of the FeZr system, one can expect some changes in T_C(AM) and the hyperfine field as well, characteristic of the new amorphous matrix as compared with the as-quenched Fe(Cu)ZrB alloy.

(iii) Exchange magnetic interactions between isolated crystals are enabled to occur through the ferromagnetic contribution of a certain portion of atoms inside the amorphous matrix which are, in turn, enhanced by the newly established ferromagnetic coupling among the crystalline grains.

Because of the rather small crystalline fraction in the present samples, the increase of the magnetic ordering temperature of the AM phase is essentially due to structural and stress relaxation effects and to some extent to the first chemical changes within the AM phase. Nevertheless, magnetic exchange interactions may influence a small content of iron nuclei located in the close neighbourhood of the crystallites: such a feature may explain the occurrence of a small tail in the high-Δ-value region of the corresponding $P(\Delta)$ distribution (namely, at 348 K in figure 5(b)), and the temperature range of the magnetic ordering transition for annealed alloys being wider than that for the as-quenched alloys.

The isolated crystals mainly act as chemical inhomogeneities within the amorphous remainder; this is manifested by differences between the isomer shifts of the AM components for $x = 0$ (open circles) and $x = 1$ (solid circles) in figure 6(a). When $x = 1$, the isomer shift values of the IF zone are closer to those of α-Fe crystals, plotted as triangles; this indicates the close similarity of resonant atoms located in CR and IF structural positions.

The fact that the values of H_{eff} for the IF component are lower than those for the CR component in figure 6(b) (solid squares and triangles, respectively) can be explained by the disordered arrangement of IF atoms and their neighbourhoods in the grain boundaries. Consequently, the IF subspectrum is treated using distributions of hyperfine magnetic fields for the samples annealed at higher temperatures where the IF contribution is more pronounced.

Table 1. Relative contributions of the amorphous residual phase (AM), interface zone (IF), and crystalline phase (CR), and the ratio of IF to CR as derived from Mössbauer spectra of $Fe_{87.5-x}Cu_xZr_{6.5}B_6$ alloys treated for one hour at the annealing temperature t_a. The figures presented were obtained by averaging the results of Mössbauer effect measurements performed at 6–8 different measuring temperatures. The statistical errors of the last digit are given in brackets.

x (% Cu)	t_a (°C)	AM (%)	IF (%)	CR (%)	IF/CR
0	500	99(1)	—	1.0(5)	—
	600	36.5(9)	18.2(14)	46.3(7)	0.39(3)
	700	26.6(7)	18.2(17)	55.2(10)	0.33(4)
	840	7.0(6)	9.6(18)	79.8(11)	0.12(2)
	840	—	—	3.6(7)	—
1	500	94.5(4)	3.1(5)	2.4(8)	1.3(5)
	600	34.3(9)	25.7(10)	40.0(4)	0.64(3)
	700	26.6(9)	23.6(12)	49.8(5)	0.48(3)
	840	8.3(4)	6.9(3)	83.7(3)	0.08(1)
	840	—	—	1.1(3)	—

Mössbauer spectra taken above T_C(AM) are characterized by a well developed central quadrupolar doublet upon which traces of magnetic sextets can be seen (figure 5). At these measuring temperatures, magnetic particles exist within a paramagnetic amorphous matrix. Because of the small size of the nanocrystals [25] and the sufficiently thick intergranular matrix, which constitutes an overwhelming volume fraction (see table 1 above) in both types of sample, superparamagnetic behaviour of the ensemble of

nanocrystalline particles is expected at high temperature. This was, indeed, recently confirmed for $Fe_{66}Cr_8Cu_1Nb_3Si_{13}B_9$ [3] and $Fe_{72}Cu_1Nb_{4.5}Si_{13.5}B_9$ [26, 27] alloys using magnetic measurements. At elevated temperatures of measurement, thick paramagnetic layers minimize the magnetic interactions among ferromagnetic nanocrystals. As a consequence, a decrease in H_{eff} is observed in the CR component with respect to the H_{eff}-value of pure α-Fe [28] especially at elevated temperatures of measurement but also at room temperature where the AM phase is still not fully magnetic. This was also observed in [11, 12] where the decrease of H_{eff} for the crystalline component was considered to be due to the phase not being a pure α-Fe one. We speculate that superparamagnetic behaviour of the α-Fe nanoparticles may be responsible for the observed effect. Changes in the character of the hyperfine interactions are manifested also by increased value of the FWHM of the corresponding sextet at elevated temperatures of measurement, for which the influence of the paramagnetic surrounding on the magnetic state of isolated nanocrystals is enhanced. No higher-temperature Mössbauer spectra could provide more information, because the measurement time leads to structural evolution of the nanocrystalline alloy. Nevertheless, in-field high-temperature Mössbauer experiments (350 K $< T <$ 400 K) have to be performed to check that superparamagnetic behaviour is occurring.

It was reported [9, 17, 25] that the presence of Cu in Fe(Cu)ZrB alloys influences the crystallization process not only by decreasing the crystallization temperature, but also by limiting the size of the α-Fe grains, which are more spherical in shape than the dendritic α-Fe crystals observed in nanocrystallized alloys without Cu. Because of the irregular shapes of the crystals in the $x = 0$ samples, the distances between neighbouring nanocrystals are smaller in certain regions, thus suppressing the superparamagnetic behaviour. The respective H_{eff}-values in figure 6(b) (open triangles) are closer to the values for pure α-Fe.

The effect of magnetic interactions among isolated α-Fe nanocrystals through paramagnetic layers as described e.g. in [4] is clearly evident in the Mössbauer spectra of the $Fe_{86.5}Cu_1Zr_{6.5}B_6$ ($x = 1$) partially crystallized alloy shown in figure 5(b) and the related parameters shown in figure 6. While the as-quenched sample is fully paramagnetic at 348 K (figure 3), the nanocrystalline sample obtained after a 500 °C/1 h annealing exhibits a considerable contribution from magnetic dipole interactions at this measuring temperature as manifested by a tail in the high-Δ-value region of the corresponding $P(\Delta)$ distribution in figure 5(b). The transition to a paramagnetic state proceeds over a wider temperature range for the annealed alloy than for the as-quenched alloy.

Propagation of magnetic dipole interactions into the paramagnetic AM phase is evident from the higher average quadrupolar splitting values in figure 6(b) (the right-hand y-axis, solid circles) for $x = 1$ than for $x = 0$ or $x = 1$ in the as-quenched state as shown in figure 4(b). These values are, however, decreasing with rising temperature of measurement when electric quadrupolar interactions start to dominate. The same trend is observed for the standard deviations of $P(\Delta)$ shown in figure 6(c) (the right-hand y-axis) where the differences between the results for the sample without and with Cu are more apparent.

4.2.3. The first stage of crystallization. Heat treatment at temperatures of 600 °C and 700 °C for one hour leads to the appearance of well resolved sextets attributed to α-Fe. Examples of Mössbauer spectra for $x = 0$ are shown in figure 7. They were fitted by the procedure described in [6], and the $P(H)$ distributions obtained are plotted on the right-hand side of each panel for the AM and IF phases. The hyperfine fields of the AM phase adopt H-values from 0 T to about 25 T, and those of the IF zone range from about 20 T to 35–37 T depending on the temperature of measurement. The vertical lines in $P(H)$

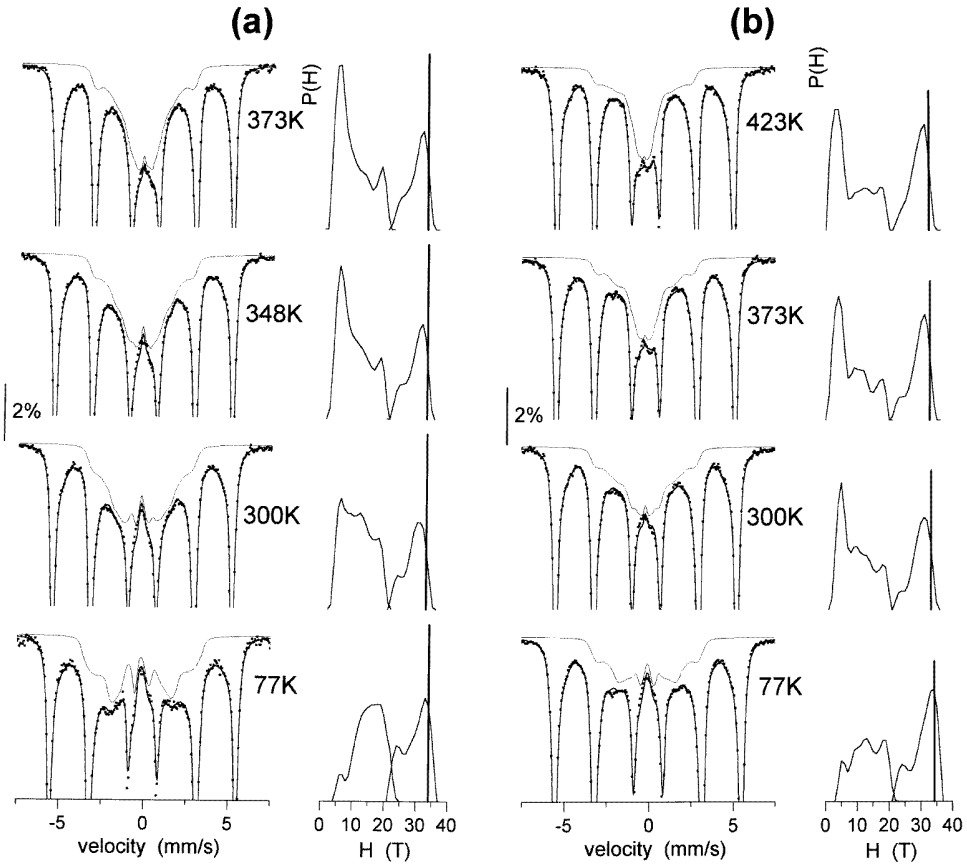

Figure 7. Mössbauer spectra (left in each panel) taken at the temperatures indicated, and the corresponding distributions of magnetic hyperfine fields (right in each panel) of $Fe_{87.5}Zr_{6.5}B_6$ alloy heat treated at: (a) 600 °C/1 h; (b) 700 °C/1 h. The amorphous subspectra are given as thin solid curves. The thick vertical lines represent the ten-times-reduced hyperfine-magnetic-field values of the discrete crystalline components.

represent by their positions and intensities the hyperfine fields and relative contributions of the CR phase, respectively. Their y-scale is reduced by a factor of 10 with respect to that for the distribution components.

The parameters of the subspectra refined from the Mössbauer spectra of $Fe_{87.5-x}Cu_xZr_{6.5}B_6$ annealed at 600 °C/1 h and 700 °C/1 h are presented in figures 8 and 9, respectively.

The distributed subspectra of the AM phase are shown in figure 7 as thin solid lines. They show the presence of both magnetic dipole and electric quadrupolar interactions, especially towards high temperatures of measurement. The magnetic-to-paramagnetic transformation does not proceed over the whole bulk at the same temperature. Instead, one can find regions with different magnetic ordering temperatures. The temperature dependence of the average field of the AM phase shown in figure 8(b) exhibits this phenomenon as two different slopes. The corresponding standard deviations shown in figure 8(c) exhibit a slight increase, which also confirms the complexity of the hyperfine interactions inside the AM phase. Multiple magnetic arrangements are found especially at higher temperatures. As a

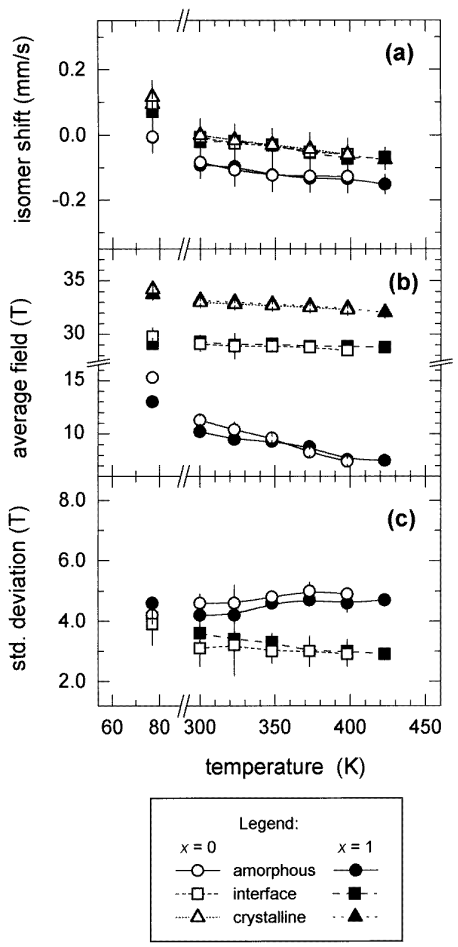

Figure 8. Parameters of the Mössbauer spectrum components (AM—circles; IF—squares; CR—triangles) plotted against the temperature of measurement for the 600 °C/1 h heat-treated $Fe_{87.5-x}Cu_xZr_{6.5}B_6$ alloys (open symbols: $x = 0$; solid symbols: $x = 1$): the isomer shift (a), and the average field (b) and its standard deviation (c).

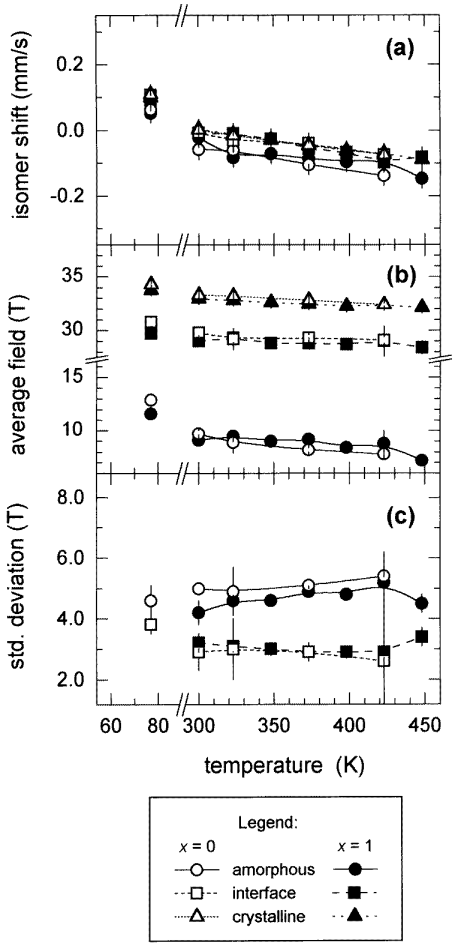

Figure 9. Parameters of the Mössbauer spectrum components (AM—circles; IF—squares; CR—triangles) plotted against the temperature of measurement for the 700 °C/1 h heat-treated $Fe_{87.5-x}Cu_xZr_{6.5}B_6$ alloys (open symbols: $x = 0$; solid symbols: $x = 1$): the isomer shift (a), and the average field (b) and its standard deviation (c).

consequence, it is not possible to determine a single T_C-value for the AM phase as a whole.

For the present samples, the exchange magnetic interactions between crystalline grains and the amorphous matrix are expected to contribute to the magnetic behaviour as a whole because of the present size of the grains, and the chemical evolution of the AM phase as well, while the structural and stress relaxation effects become negligible. The magnetic ordering temperature of the whole AM phase of this sample cannot be clearly estimated in the present temperature range of measurement; some iron nuclei still exhibit a high magnetic hyperfine field, whereas others are paramagnetic, according to their respective neighbourhoods.

The isomer shift values shown in figures 8(a) and 9(a) indicate the close similarity of

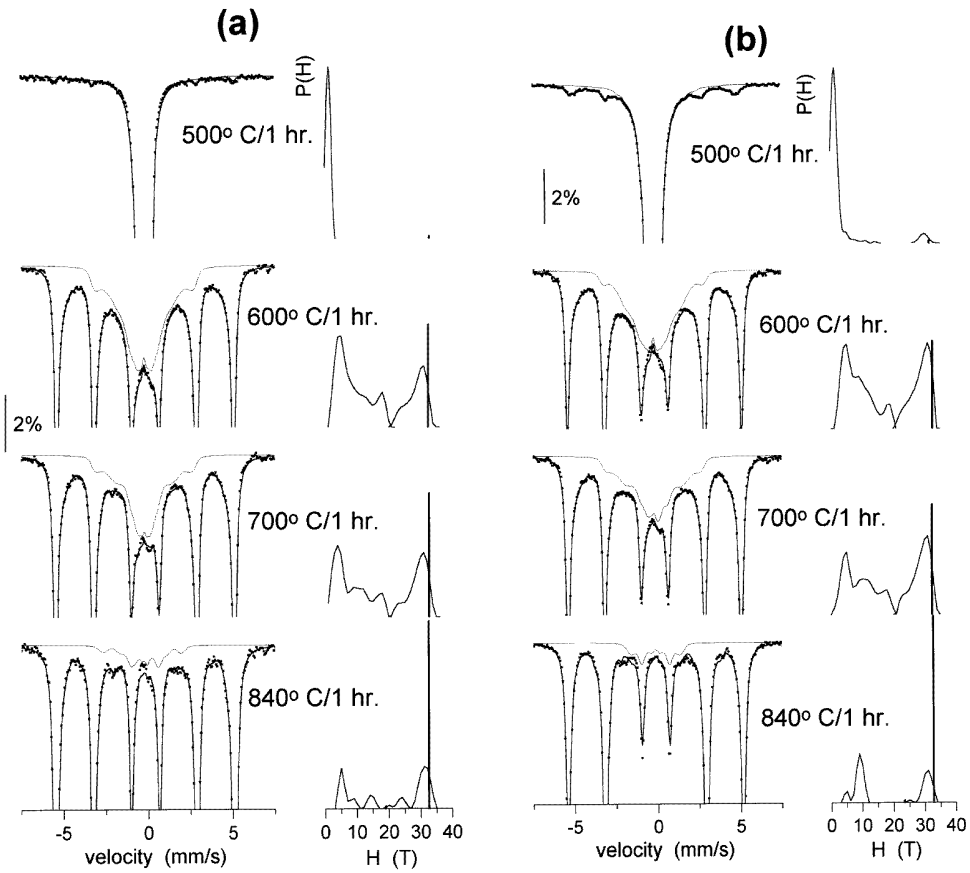

Figure 10. Mössbauer spectra (left in each panel) taken at 373 K, and the corresponding distributions of hyperfine interactions (right in each panel) of the $Fe_{87.5-x}Cu_xZr_{6.5}B_6$ alloys with: (a) $x = 0$; (b) $x = 1$, heat treated at the temperatures indicated for one hour in a vacuum. The amorphous subspectra are given as thin solid curves. The thick vertical lines represent the ten-times-reduced hyperfine-magnetic-field values of the discrete crystalline components. The AM $P(H)$ distributions for the 500 °C/1 h samples are $P(\Delta)$ distributions redrawn on the H-scale and reduced by a factor of 2.

the resonant atoms originating from CR and IF phases. The fact that the average fields of the IF phase shown in figures 8(b) and 9(b) are lower than those of the CR phase suggest that the nearest surroundings of these atoms are composed not only of Fe but also of other constituent elements of the Fe(Cu)ZrB system and/or that the coordination of Fe nearest neighbours in the IF zone varies. The latter adopts a more favourable structural arrangement at elevated temperatures of measurement, as is evident from the decreasing standard deviations in figure 8(c) and 9(c) (squares).

We cannot, however, consider the IF zone to be solely due to the presence of Zr in the first-neighbour shell of bcc-Fe atoms [9, 19], because the same IF spectral feature was also found in nanocrystalline alloys which do not contain Zr atoms [20, 21]. The main contribution to the $P(H)$ distribution of the IF zone comes from the Fe atoms located at the surfaces of nanocrystalline grains [6]. Their hyperfine fields constitute the principal $P(H)$ peak which is positioned at about 30–32 T (depending on the temperature of measurement).

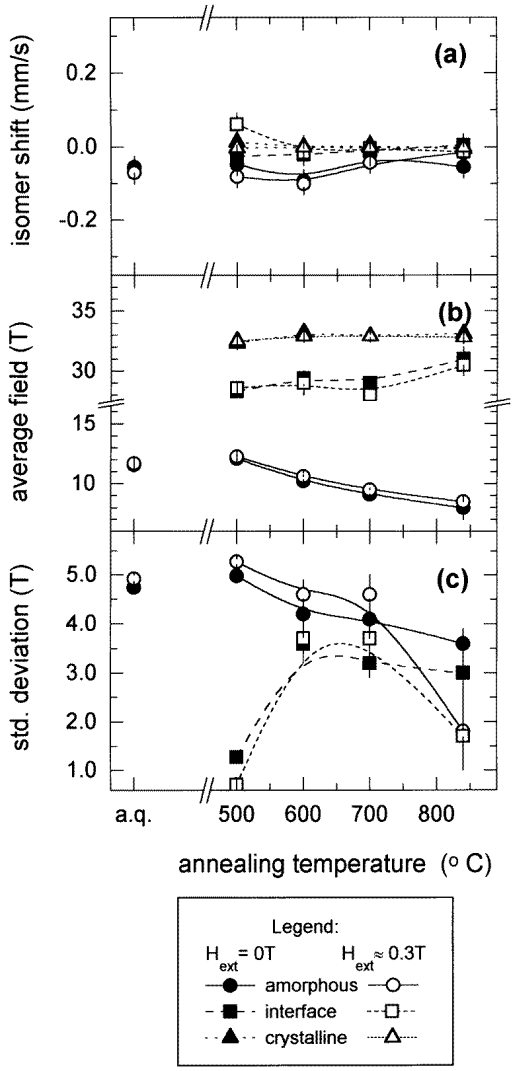

Figure 11. Parameters of the Mössbauer spectrum components (AM—circles; IF—squares; CR—triangles) plotted against the annealing temperature (treatment for one hour in a vacuum) for the $Fe_{86.5}Cu_1Zr_{6.5}B_6$ alloy measured at room temperature without (solid symbols) and with (open symbols) an external magnetic field $H_{ext} \approx 0.3$ T parallel to the ribbon plane: the isomer shift (a), and the average field (b) and its standard deviation (c).

The surface atoms have the highest probability of non-magnetic neighbours dissolved in the surrounding amorphous matrix [29]. This situation is very similar (though opposite, from the point of view of the absolute value of the hyperfine field) for the Fe atoms of the amorphous remainder which are in close contact with the nanocrystalline bcc-Fe grains. That is why the lower-field component of the IF-$P(H)$ is attributed to the latter Fe atoms.

Changes in the chemical short-range order in the IF zone during measurements at different temperatures can be excluded, because no appreciable changes are observed in the shapes of the corresponding IF-$P(H)$ distributions shown in figure 7.

4.2.4. The second stage of crystallization. As seen from the DTA curve in figure 1, the second crystallization is well developed beyond 800 °C. Mössbauer spectra of $Fe_{87.5-x}Cu_xZr_{6.5}B_6$ annealed at 840 °C/1 h resemble at first sight simple six-line patterns (see for example the bottom parts of figure 10). We have adopted the same fitting procedure as described above, comprising using two independent distribution blocks to reconstruct the AM and IF components and one CR sextet, and found it necessary to introduce another sextet of narrow lorentzian lines to account for the presence of other crystalline phases. Navarro *et al* [15] reported a 20.5% contribution of three crystalline phases (13.3 T, 17.1 T, and 24.9 T) in $Fe_{88}Zr_7B_4Cu_1$ annealed at 705 °C. Our results give $H_{\mathrm{eff}} = 19.2$ T and 23.9 T (at 300 K) for $x = 0$ and $x = 1$ with percentages of 4% and 1%, respectively. The differences in the fractions of the additional crystalline phases determined stem from the different compositions of the samples investigated as well as from the different fitting procedures involved. It is speculated from x-ray diffraction results [17] that the crystalline phase in our samples can be ascribed to Fe–Zr and/or Fe–B.

To demonstrate the reliability of the fitting procedure, in figure 10 we provide Mössbauer spectra of samples with $x = 0$ and $x = 1$ thermally treated at 500, 600, 700, and 840 °C/1 h which were taken at 373 K. AM subspectra are plotted in each section as thin solid lines. It can be seen from the accompanying $P(H)$ distributions that the same qualitative shapes of $P(H)$ curves are obtained for the AM and IF phases for each specimen. They will be discussed in more detail later in this paper. It should be noted that the low-field curves in the $P(H)$ plots of samples annealed at 500 °C are in fact $P(\Delta)$ distributions corresponding to the AM phase which have be redrawn using the H-scale for the sake of comparison. Their vertical scale is reduced by a factor of 2 with respect to those for other $P(H)$ distributions. The scale for the thick vertical lines which represent the discrete H_{eff}-values of the CR components is reduced by a factor of 10.

To minimize the effects of line overlap, we have performed measurements in external magnetic fields ($H_{\mathrm{ext}} \approx 0.3\ T$) oriented parallel to the plane of the ribbon-shaped absorbers. This enabled us to introduce simplifying constraints into the fitting procedure as regards the line intensity ratio (3:4:1:1:4:3). The spectral parameters derived from the room temperature Mössbauer spectra taken without and with an external magnetic field are plotted in figure 11 as solid and open symbols, respectively. The values of the isomer shifts and standard deviations of the $P(H)$ distributions are almost the same within the experimental errors, as expected. The slight decrease of the average field values for the in-field CR and IF components shown in figure 11(b) is due to the complete alignment of the magnetic moments in the plane of the ribbon-shaped absorbers. The opposite tendency is observed for the AM component. As documented by figure 12, in which the $P(H)$ distributions of the AM and IF spectral components are plotted for in-field and out-of-field Mössbauer spectra as dotted and solid lines, respectively, the same characteristic features of the distributions are observed. The positions of the individual $P(H)$ peaks are shifted towards lower H-values for the in-field experiments due to the above-mentioned effect of magnetic moment alignment. Deviations in the peak intensities give rise to higher average H-values for the in-field spectra.

The relative areas of the AM, IF, and CR spectral components are summarized in table 1 for all of the thermal treatments. The figures presented were obtained by averaging 6–8 values from the fits of the spectra taken at different measuring temperatures. No constraints were involved in the fits as regards the extents of the contributions of the individual subspectra. Statistical errors, giving the deviations in the last digit, are also provided to enable an estimation of the dispersion in the area values to be made. The last column in table 1 gives an IF/CR ratio which can be regarded as the raw ratio of the number

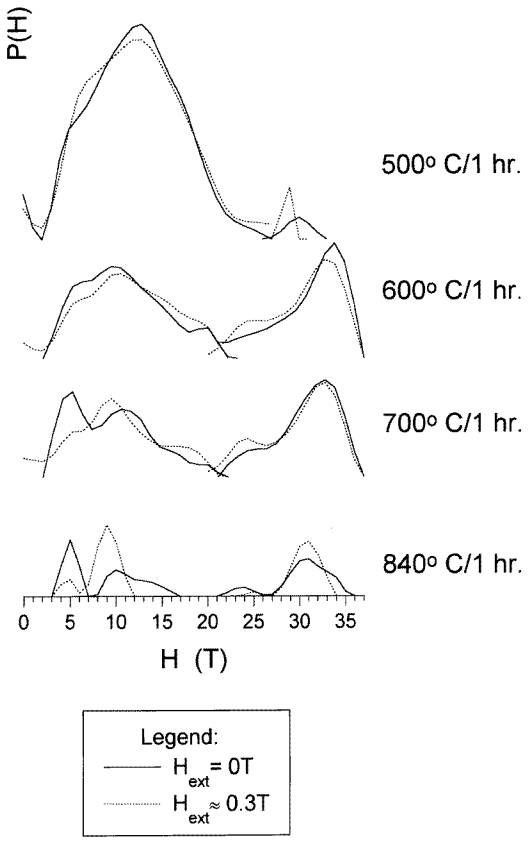

Figure 12. Distributions of the hyperfine magnetic fields of the $Fe_{86.5}Cu_1Zr_{6.5}B_6$ alloy annealed for one hour at the temperatures indicated in a vacuum, and measured at room temperature without (solid line) and with (dotted line) an external magnetic field $H_{ext} \approx 0.3$ T parallel to the ribbon plane.

of atoms localized in the surface to that in the bulk of α-Fe crystals. The second row for 840 °C/1 h annealed samples shows the relative contributions of other crystalline phases revealed during the second crystallization step. Their fractions are rather small, and this coincides with the findings from x-ray diffraction measurements performed upon the same samples (figure 2).

4.2.5. The distribution of hyperfine fields. Utilization of the fitting procedure with separate blocks of hyperfine-field distributions for different spectral components, namely for the AM and IF phases, and discrete sextets of CR subspectra [6], enables a detailed investigation to be made of the hyperfine interactions and/or structural sites of the resonant atoms. With the aim of better visualizing the information obtained from the $P(H)$ distributions, we present their three-dimensional (3-D) mappings. The latter are plotted by stacking $P(H)$ distributions corresponding to a particular temperature of measurement in the same image. In this way, the measuring temperature establishes the second dimension of the 3-D images, and allows a quantitative and qualitative comparison of the $P(H)$ distributions.

3-D $P(H)$ mappings corresponding to the amorphous remainders and interface zones

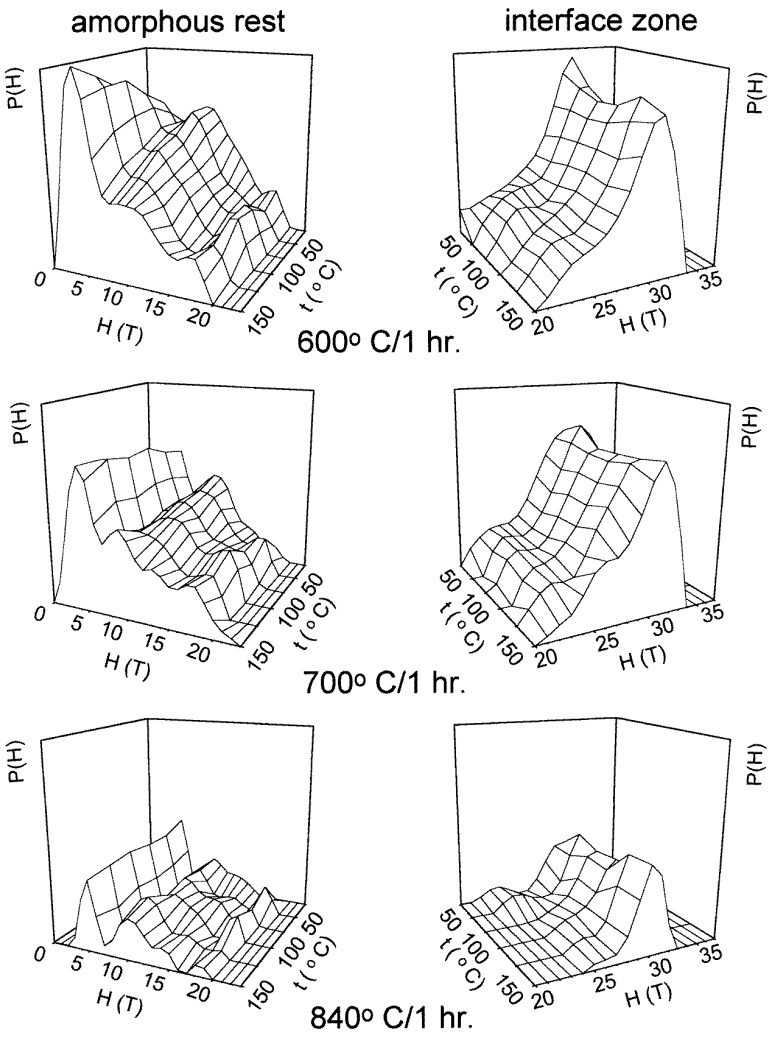

Figure 13. A three-dimensional mapping of the hyperfine-magnetic-field distributions $P(H)$ of the $Fe_{86.5}Cu_1Zr_{6.5}B_6$ alloy heat treated for one hour at the temperatures indicated in a vacuum, corresponding to the amorphous residual phase (left) and to the interface zone (right). The temperature of measurement, t, is the second dimension of the 3-D images, and ranges from 25 to 150 °C.

of $Fe_{86.5}Cu_1Zr_{6.5}B_6$ alloys annealed at 600, 700, and 840 °C/1 h are illustrated in figure 13 for temperatures of measurement, t, ranging from 25 to 150 °C (300 to 423 K). The same scales on the H-, t-, and $P(H)$-axes are used, which makes direct comparison of the $P(H)$ features for the above-room-temperature Mössbauer spectra possible.

The 3-D $P(H)$ mappings on the right-hand side of figure 13 which correspond to the interface zones exhibit obvious similarity from the qualitative point of view (shape features) for all of the heat treatments. This again supports the proposal that IF phases are not formed solely from bcc-Fe atoms with Zr nearest neighbours as declared in [9, 19]. They consist of bcc-Fe atoms positioned in grain boundaries and those Fe atoms that belong to the AM phase

but are in close contact with α-Fe nanocrystals [6, 20, 21]. Should the explanations proposed in [9, 19] be valid (apart from the fact that the same features of the IF-$P(H)$ are observed for alloys without Zr [20, 21]), we would expect qualitative changes in the shapes of the $P(H)$ distributions both with the annealing temperature and with the temperature of measurement. Different heat treatments lead to different proportions of crystalline and amorphous parts, which also means that the relative contribution of non-iron constituent elements in the AM phase varies with the annealing temperature, and this must be, therefore, consequently manifested by deviations in the shapes of the $P(H)$ distributions. The character of the $P(H)$ distributions in Fe–Zr alloys undergoes substantial changes also with the temperature of measurement [23]. Neither of these effects takes place, because no changes in the shape of the IF-$P(H)$ are observed in figure 13. Instead, only a quantitative decrease of the peak intensities is seen with elevated annealing temperature. This is associated with the decrease of the fraction of amorphous remainder with progressing crystallization.

We ascribe the lower-field tail in the IF-$P(H)$ at about 22 T to Fe atoms which originate from the AM but are facing the bcc-Fe nanocrystals. As the AM fraction decreases with annealing temperature (table 1), the relative contribution of amorphous Fe atoms with $H \approx 20$ T also decreases, and eventually vanishes for the 840 °C/1 h specimen.

As far as changes in the IF-$P(H)$ with respect to the temperature of measurement are concerned, no appreciable deviations in shape are observed. The slight shift of the peak positions toward smaller H-values is a consequence of the temperature dependence of the hyperfine magnetic fields. It is manifested by the decrease of the average fields with rising temperature of measurement shown in figures 6(b), 8(b), and 9(b).

The 3-D mappings of the AM-$P(H)$ distributions in figure 13 (left) show evident variations in the shape (quality) and intensity (quantity) of the probability peaks. They can be ascribed mainly to changes in the chemical short-range order as a consequence of the different compositions of the remaining AM phase after different stages of crystallization when the original amorphous precursor is depleted in Fe to different extents (table 1). For example, in the 840 °C/1 h sample where the AM content is very small, hyperfine fields of around 5 T are more pronounced, which indicates that the dominating Fe atoms are already in non-magnetic states even at room temperature.

The character of the hyperfine interactions within the AM component exhibits apparent changes also with the temperature of measurement. Electric quadrupolar interactions, which are represented by H-values from 0 T up to about 7 T, prevail in the 600 °C/1 h sample above 100 °C (373 K), i.e., beyond the magnetic ordering temperature of the AM phase. As seen from the 3-D mappings, some proportion of the Fe atoms are still in magnetic sites.

We can find some common features of the AM-$P(H)$ and IF-$P(H)$ distributions which can be generalized for all samples regardless of the annealing conditions and/or temperature of measurement. To discuss them, we will use the $P(H)$ distributions of the $Fe_{86.5}Cu_1Zr_{6.5}B_6$ alloy annealed at 600 °C/1 h and measured at 373 K (100 °C) as an example; these are presented in figure 14. The AM-$P(H)$ can be decomposed into three gaussian components positioned at about 5 T, 10 T, and 18 T. Similarly, the IF-$P(H)$ component shows a clear bimodal feature which is also reproduced by one gaussian at about 22 T and a pair of gaussians close to one another as seen in the upper part of figure 14. We have already discussed the origin of the lower-field tail in the IF-$P(H)$—it is due to amorphous Fe atoms which are touching the outer surfaces of bcc-Fe crystalline grains. The high-field part of the AM-$P(H)$ represents Fe atoms located in the 'outer surface' of the amorphous precursor which are also very close to the crystallites. From the point of view of hyperfine interactions, the two kinds of Fe atom are indistinguishable. It is only a consequence of the fitting procedure (separation of a single-block $P(H)$ into two

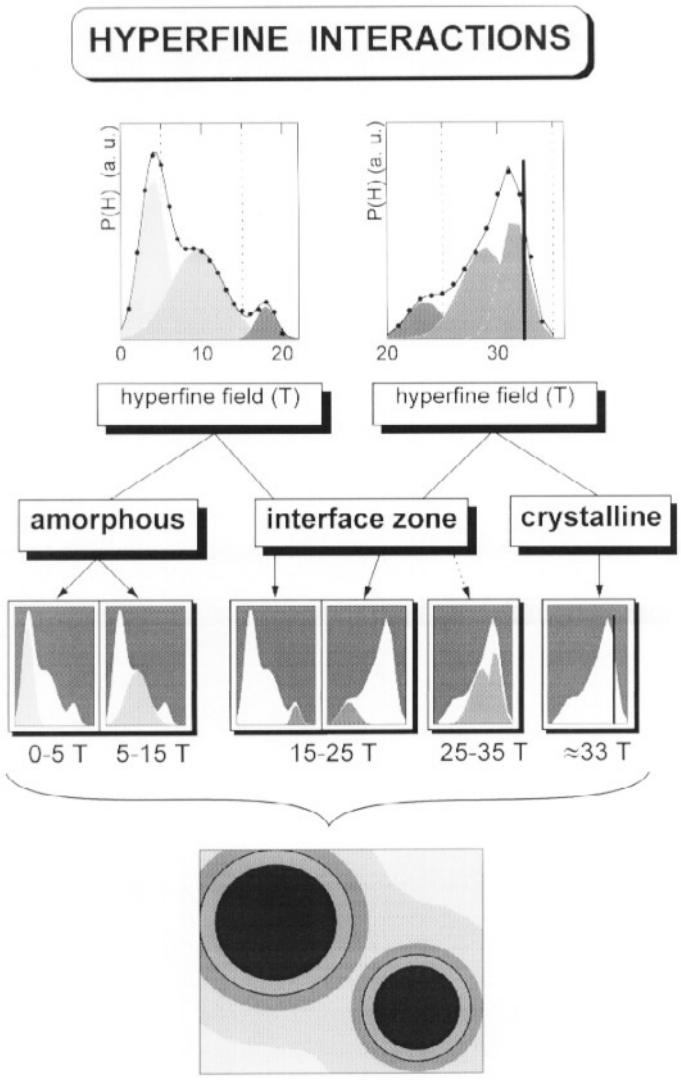

Figure 14. The distributions of the hyperfine magnetic fields for the 600 °C/1 h heat-treated $Fe_{86.5}Cu_1Zr_{6.5}B_6$ alloy measured at 373 K (top), and their decomposition into gaussian components (middle). Also given is a schematic model of the topography of the hyperfine interactions (bottom) as derived from the $P(H)$ decompositions.

independent parts [6]) that they belong to the upper and lower limits of the AM and IF components, respectively. But their hyperfine-field values are very alike, anyway.

The decomposition of the AM-$P(H)$ and IF-$P(H)$ distributions into gaussian components, and their relationship to the structural phases is shown schematically in the middle part of figure 14. As seen from this representation, in order to derive the ratio of amorphous and crystalline parts in a nanocrystalline sample, we have to decompose the IF component into its 'amorphous' (≈25 T) and 'crystalline' (≈25 to 35 T) parts and then add together the latter (which in fact represents the Fe atoms in the grain boundaries) and the

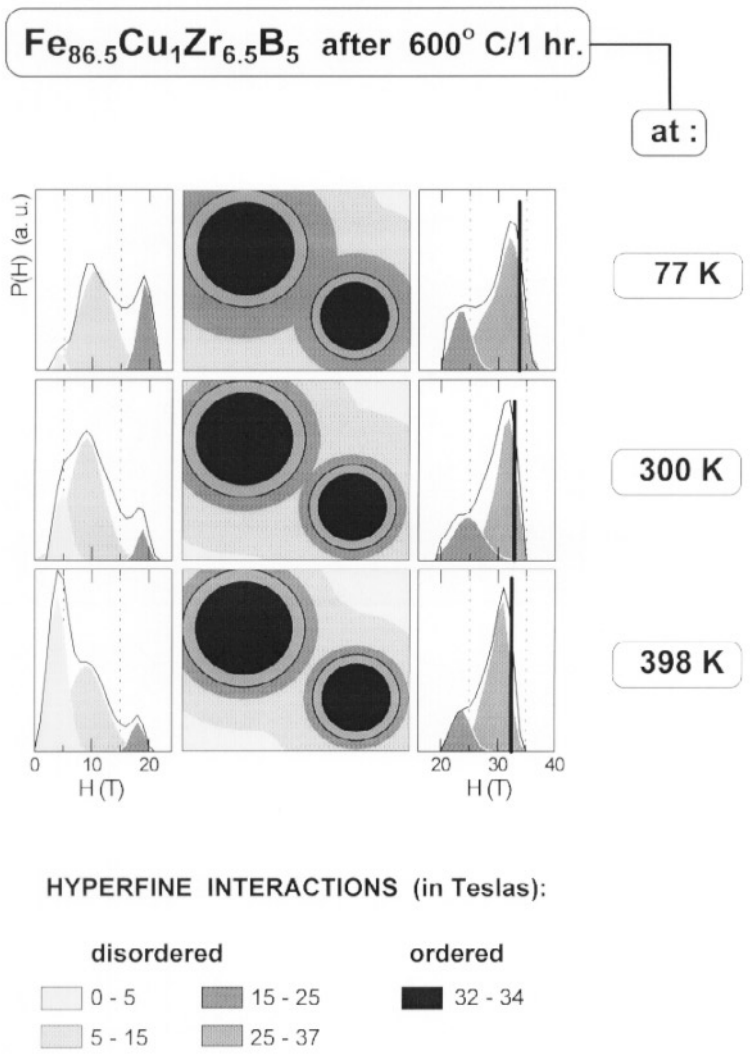

Figure 15. The topography of the hyperfine interactions and $P(H)$ distributions of the AM (left) and IF (right) phases derived from the Mössbauer spectra of the 600 °C/1 h heat-treated $Fe_{86.5}Cu_1Zr_{6.5}B_6$ alloy measured at the temperatures indicated.

area of the α-Fe crystalline sextet contribution.

The bulk amorphous phase is in general characterized by low (0–5 T) and medium (5–15 T) hyperfine fields. The former are electric quadrupolar interactions which refer to Fe atoms in non-magnetic positions. Their relative content is changing mainly with the temperature of measurement on account of the medium-field component, as is evident from figure 13 (left). Since for enhanced annealing temperatures more Fe atoms segregate into the crystalline phase, the amorphous residuum is enriched in non-magnetic constituent elements, which is consistent with an increase of the low-field AM-$P(H)$ peak. At the same time, the amorphous phase becomes more stable as the temperature of measurement is varied, too. It is possible to reproduce the spectral part corresponding to the low fields with distributions

of quadrupolar splitting values, as discussed in [6] in more detail.

The high-field peak of the AM-$P(H)$ (15–25 T) does not show substantial changes in intensity with the temperature of measurement. Only a slight shift in its position toward lower H-values, due to the temperature dependence of the magnetic fields, is observed. This is indirect evidence that these atoms can be considered as belonging to an interface zone, because their magnetic states are preserved due to the proximity of the high magnetic fields of nanocrystals.

4.3. The topography of hyperfine interactions

The decomposition of the AM-$P(H)$ and IF-$P(H)$ distributions into gaussian components also gives relative contributions of the hyperfine interactions from the different regions of H-values. This information can be used to model the spreading of hyperfine interactions within a nanocrystalline material, i.e. to design the topography of hyperfine interactions, as seen in the bottom part of figure 14. The bulk of the nanocrystalline grains is schematically indicated by circles surrounded by other circles which represent the grain boundary. The hyperfine fields of the latter are typically in the range 25–35 T. The nanocrystalline grains are in this schematic representation separated from the amorphous residual precursor by thin solid lines which also indicate the outer boundary of the ordered structure.

The evolution of the hyperfine interactions with the temperature of measurement is sketched in figure 15 for a $Fe_{86.5}Cu_1Zr_{6.5}B_6$ alloy which has been thermally treated at 600 °C for one hour. The $P(H)$ distributions corresponding to the AM (left) and IF (right) components as obtained from the Mössbauer spectra are also displayed. The hyperfine-field values of the CR component are shown by thick vertical lines with a ten-times-reduced scale.

Because the size of the nanocrystals does not change with the measuring temperature, the contribution of the hyperfine fields corresponding to the grain boundaries (25–35 T) does not change either, and the corresponding hyperfine interactions occupy a constant space around the bulk of the nanocrystals. The IF-$P(H)$ distributions reflect this by the principal peak area being virtually unchanged. The low-field peak in the IF-$P(H)$ as well as the high-field one in the AM-$P(H)$ are temperature dependent, showing the highest contribution at 77 K. Consequently, hyperfine interactions from the range 15–25 T are spread out well around the nanocrystals at low temperature, but they shrink to the immediate vicinity of grains as the temperature of measurement is increased.

On the other hand, Fe atoms in non-magnetic positions start to prevail with rising temperature of measurement. Eventually, at 398 K the transformation from the magnetic to the paramagnetic state is well advanced. It is noteworthy that T_C(AM) for the 500 °C/1 h heat-treated $Fe_{86.5}Cu_1Zr_{6.5}B_6$ nanocrystal was determined to be about 360 K. Due to the magnetic coupling of α-Fe crystallites and the propagation of ferromagnetic exchange interactions through the amorphous layers [4, 5], the magnetic transition is still not fully completed in the 600 °C/1 h sample even at 398 K. The higher relative proportion of α-Fe grains and the smaller intergranular distances are responsible for the observed behaviour. The enhancement of T_C is an intrinsic property of nanoscale heterogeneous systems in which the macroscopic magnetic properties are governed by the degree of coupling between different magnetic phases [30].

The exchange coupling between nanocrystalline grains through the amorphous layers is illustrated in figure 16 where the topography of the hyperfine interactions is shown for the $Fe_{86.5}Cu_1Zr_{6.5}B_6$ nanocrystal as a function of the annealing temperature. The Mössbauer spectra were recorded at 373 K and the corresponding AM-$P(H)$ and IF-$P(H)$ distributions

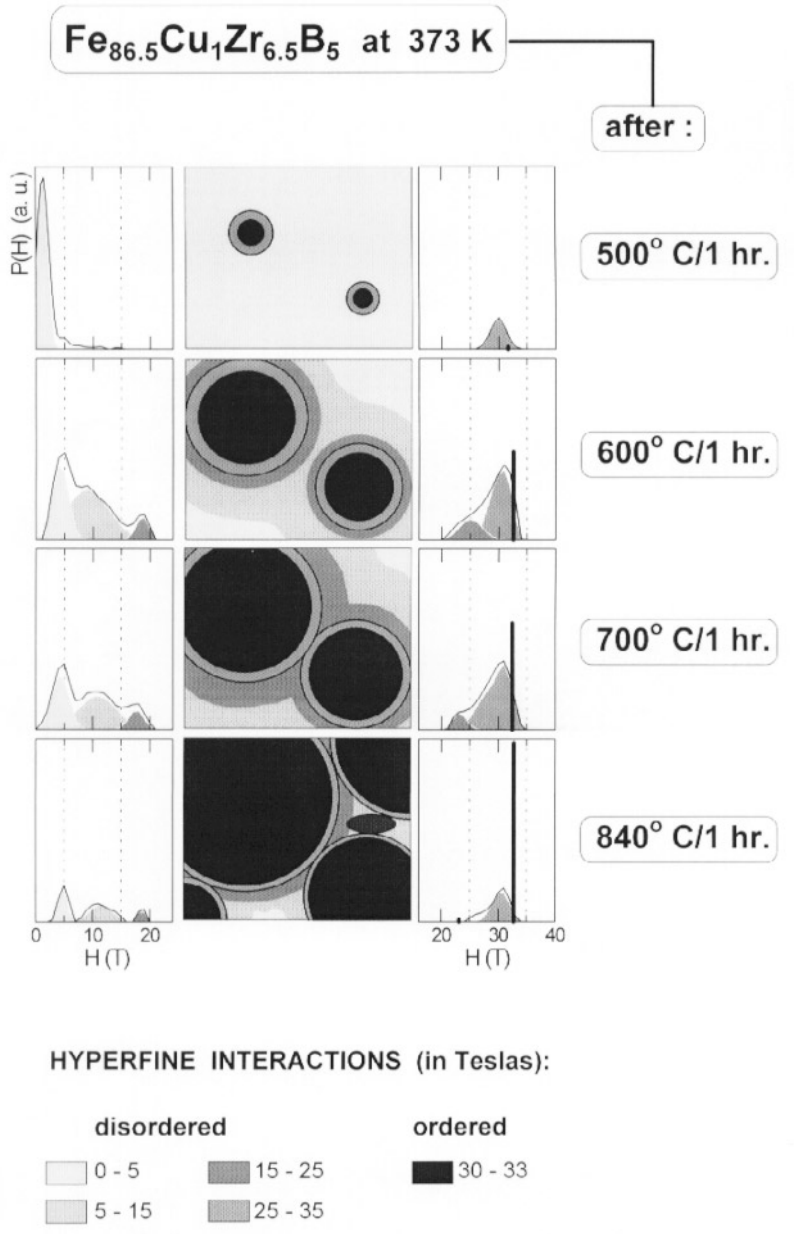

Figure 16. The topography of the hyperfine interactions and $P(H)$ distributions of the AM (left) and IF (right) phases derived from the Mössbauer spectra measured at 373 K for the $Fe_{86.5}Cu_1Zr_{6.5}B_6$ alloys heat treated at the temperatures indicated for one hour in a vacuum.

are also given. The AM-$P(H)$ of the 500 °C/1 h heat-treated alloy is in fact a $P(\Delta)$ distribution redrawn on the H-scale to allow direct comparison, and it is, like in figure 10, reduced by a factor of 2 on the $P(H)$ axis.

The scarcity of the α-Fe nanocrystals (table 1) and the smallness of their dimensions prevents any coupling among them from occurring at this measuring temperature, and

the AM phase is completely paramagnetic. The segregation of Fe atoms from the original amorphous phase and the progressive crystallization due to the increasing annealing temperature decreases the intergranular distances because of the increased grain content (table 1), and size [25]. The surface-to-bulk ratio of the α-Fe crystals changes (IF/CR in table 1) and this affects the spreading of the hyperfine interactions from the 25–35 T range. As the degree of crystallization increases one finds a smaller fraction of Fe atoms in paramagnetic states.

5. Conclusions

The fitting procedure introduced in part I, the previous paper [6], opens up new possibilities for the utilization of Mössbauer spectrometry in the study of iron-based nanocrystalline alloys. The extended Mössbauer effect study performed over a wide temperature range for $Fe_{87.5-x}Cu_xZr_{6.5}B_6$ ($x = 0, 1$) alloys at different stages of crystallization as well as the utilization of an elaborate fitting procedure and 3-D $P(H)$ mappings lead to the following conclusions. In the early stage of crystallization of $Fe_{87.5-x}Cu_xZr_{6.5}B_6$ alloys, small amounts of α-Fe nanocrystals are isolated from one another by the prevailing paramagnetic amorphous residual phase. The sizeable increase of the Curie temperature of the AM phase observed for low annealing temperature may be essentially due to both structural and stress relaxation effects within the amorphous phase. With the crystallization proceeding at elevated temperatures, the proportion of crystalline phase grows, and the intergranular distances become smaller. The decreased fraction of amorphous matrix leads to a rising proportion of atoms with higher magnetic fields due to the propagation of ferromagnetic exchange interactions through the paramagnetic layers [4, 5]. A significant role in this process is played by the atoms located in the grain boundaries of crystals and atoms of the amorphous matrix in their immediate vicinity. The relative content of atoms inside this interface zone is nearly stable during the first stage of crystallization, because the size of the grains does not exhibit a substantial change.

The transition to the paramagnetic state of the amorphous residual phase proceeds over a wide temperature range as a consequence of the enhanced number of Fe atoms with higher hyperfine fields. That is why it is not possible to determine a single value of the Curie temperature, and instead we observe a transition interval.

The decomposition of the $P(H)$ distributions of the amorphous residual phase and the interface zone into gaussian subcomponents gives the relative contributions of the hyperfine interactions with respect to their values. This in turn enables one to sketch a schematic model of the topography of the hyperfine interactions within the $Fe_{86.5}Cu_1Zr_{6.5}B_6$ nanocrystal as related to the annealing temperature and temperature of measurement. The results obtained support the theoretical predictions concerning the propagation of ferromagnetic exchange interactions between the nanocrystals through the amorphous layers as well as an increase in T_C(AM) due to this effect.

Acknowledgments

The as-quenched amorphous $Fe_{87.5-x}Cu_xZr_{6.5}B_6$ ($x = 0, 1$) alloys were provided by courtesy of Dr P Duhaj and Dr P Švec (Bratislava). The authors thank A-M Mercier (Le Mans) for her technical assistance with the x-ray diffraction measurements, and H Duroy (Le Mans) for her help with the differential thermal analysis. MM is indebted to the Région Pays de la Loire for financial support.

References

[1] Makino A, Inoue A, Hatanai T and Bitoh T 1997 *Mater. Sci. Forum* **235–238** 723–8
[2] Suzuki K, Makino A, Inoue A and Masumoto T 1991 *J. Appl. Phys.* **70** 6232–7
[3] Šlawska-Waniewska A, Gutowski M, Lachowicz H K, Kulik T and Matyja H 1992 *Phys. Rev.* B **46** 14 594–7
[4] Hernando A and Kulik T 1994 *Phys. Rev.* B **49** 7064–7
[5] Navarro I, Ortuño M and Hernando A 1996 *Phys. Rev.* B **53** 11 656–60
[6] Miglierini M and Greneche J M 1997 *J. Phys.: Condens. Matter* **9** 2303–19
[7] Kopcewicz M, Grabias A and Nowicki P 1995 *Nanostruct. Mater.* **6** 957–60
[8] Kopcewicz M, Grabias A and Nowicki P 1995 *J. Magn. Magn. Mater.* **140–144** 461–2
[9] Kopcewicz M, Grabias A, Nowicki P and Williamson D L 1996 *J. Appl. Phys.* **79** 993–1003
[10] Kopcewicz M, Grabias A and Nowicki P 1997 *Mater. Sci. Eng.* at press
[11] Gorría P, Orúe I, Plazaola F, Fernández-Gubieda M L and Barandiarán J M 1993 *IEEE Trans. Magn.* **29** 2682–4
[12] Orúe I, Gorría P, Plazaola F, Fernández-Gubieda M L and Barandiarán J M 1994 *Hyperfine Interact.* **94** 2199–205
[13] Barandiarán J M, Gorría P, Gómez Sal J C, Fernández-Barquín L and Kaul S N 1994 *IEEE Trans. Magn.* **30** 4776–8
[14] Barandiarán J M 1994 *Phys. Scr.* T **55** 194–8
[15] Navarro I, Hernando A, Vázquez M and Yu Seong-Cho 1995 *J. Magn. Magn. Mater.* **145** 313–8
[16] Gómez-Polo C, Holzer D, Multinger M, Navarro E, Agudo P, Hernando A, Vázquez M, Sassik H and Grössinger R 1996 *Phys. Rev.* B **53** 3392–7
[17] Duhaj P, Mat'ko I, Švec P, Sitek J and Janičkovič D 1996 *Mater. Sci. Eng.* B **39** 208–15
[18] Miglierini M, Tóth I, Sitek J and Lipka J 1996 *Proc. 'ICAME-95', Int. Conf. on Applications of the Mössbauer Effect (Rimini, Italy, 1995)* vol 50, ed I Ortalli (Bologna: Italian Physical Society) pp 417–20
[19] Kemény T, Varga L K, Kiss L F, Balogh J, Lovas A and Vincze I 1997 *Mater. Sci. Eng.* at press
[20] Miglierini M and Greneche J M 1997 *Czech. J. Phys.* at press
[21] Škorvánek I, Miglierini M and Duhaj P 1997 *Mater. Sci. Forum* **235–238** 771–6
[22] Brand R A 1989 *NORMOS program* 1989 version, unpublished
[23] Nasu S, Miglierini M, Kitagawa H and Fukamichi K 1994 *Hyperfine Interact.* **84** 177–81 and references therein
[24] Ryan D H, Coey J M D, Batalla E, Altounian Z and Ström-Olsen J O 1987 *Phys. Rev.* B **35** 8630–8
[25] Šlawska-Waniewska A and Nowicki P 1995 *Mater. Sci. Forum* **179–181** 563–8
[26] Škorvánek I and O'Handley R C 1995 *J. Magn. Magn. Mater.* **140–144** 467–8
[27] Škorvánek I, Kim C K and O'Handley R C 1995 *Science and Technology of Rapid Solidification and Processing* ed M A Otoani (Dordrecht: Kluwer Academic) pp 309–16
[28] Preston R S, Hanna S S and Heberle J 1962 *Phys. Rev.* **128** 2207–18
[29] Greneche J M and Slawska-Waniewska A 1997 *Mater. Sci. Eng.* at press
[30] Hernando A, Navarro I, Prados C, García D, Vázquez M and Alonso J 1996 *Phys. Rev.* B **53** 8223–6